TECHNICAL PAPER

Analysis of fatigue crack growth in cylinder head bolts of gasoline engine based on experimental data

Karim Aliakbari[1] · Tohid Akbarpour Mamaghani[1]

Abstract

Engines cylinder head bolts failure from the thread location in cylinder block causes the problems during repairing time. Exact prediction of fatigue crack growth in bolts by experimental analysis and finite element method modeling can affect the Maintenance Planning and Scheduling Implementation. In this study, the fatigue analysis of cylinder head bolts of a four-cylinder gasoline engine imposed by premature failure is investigated. The bolts suffer a mechanical seizure on the threads about 2×10^8 cycles in service. For such aim, standard specimens are cut off from the bolts and examined to evaluate the mechanical properties and material chemical composition. Optical microscopes and scanning electron microscopy are employed to consider the microstructures, defects, fracture surface and failure cause. The morphology of the fracture surface shows the fatigue crack growth marks, including the beachmarks, the ratchet marks and the river cracks. The finite element analysis model is presented applying the elastic–plastic finite element analysis for the bolts under variable combustion pressure. The stress history is then used to calculate stress intensity factors and fatigue life of bolts. Numerical results show that crack existence to depth of 0.35 mm is the source of failure of premature fracture.

Keywords Cylinder head bolt · Finite element analysis · Stress intensity factor · Fatigue life · Failure cause

Abbreviations

HV	Vickers hardness (HV)
F_G	Maximum gas force (N)
F_{PT}	Pre-tightening force (N)
F_T	Force generated by the engine heat (N)
A_{Cyl}	Cylinder area (m²)
K_I	Stress intensity factor (MPa.m$^{0.5}$)
F_I	Boundary correction factor (−)
B_S	Applied tensile stress (MPa)
K_{max}	Maximum mode I stress intensity factor (MPa.m$^{0.5}$)
K_{op}	Crack first opens (MPa.m$^{0.5}$)
ΔK_{eff}	Effective stress intensity factor (MPa.m$^{0.5}$)
C	Material constant (m/cycle)
n	Material constant (−)
k	Nut factor
i	Number of cylinder head bolts per any cylinder
N	Fatigue life (cycle)
a_0	Crack initial length (m)
a_f	Crack final length (m)

Greek letters

α	Correction coefficient
$\emptyset$	Parametric angle
σ	Stress (Pa)

Subscripts

G	Gas
Cyl	Cylinder
f	Final
tot	Total
max	Maximum
eff	Effective
p	Proposed

✉ Karim Aliakbari
karim.aliakbari@gmail.com

1 Department of Mechanical Engineering, Faculty of Montazeri, Khorasan Razavi Branch, Technical and Vocational University (TVU), Mashhad, Iran

1 Introduction

Cylinder head bolts failure in automobile engines occurs due to various factors such as excessive torque applied to bolts, bolts fatigue, corrosion effect, thermal residual stresses in bolts, inappropriate material and unsuitable connection when bolts are inserted into cylinder blocks. The initiation

of the crack and cracks growth occur in the threads, which are the stress concentration points. Accordingly, the identification of these points and the amount of stresses in these points can be very useful for research with nondestructive tests and fatigue life estimation methods [1, 2].

Fonte et al. [3] analyzed failure analysis of the cylinder head studs used in the marine main engine. Calculations of the studs pre-tightening showed that cause of failure was a significant high stress concentration mainly at the second thread root of the studs, close to the bottom side of the nut. Yu and Xu [4] analyzed the cylinder head bolts failure analysis used in the diesel engine of the truck. Fracture in the smooth rod and threaded end sections was occurred during initial tightening. Studies of failure surface and metallurgy showed that the fracture surfaces and microstructure of the two failed bolts have similar characteristics, and the fracture surfaces showed the fracture of cleavage and quasi-cleavage characteristics.

Aliakbari [5] investigated the failure analysis of base plate bolts of radial forging machine. Stress analysis indicated that the amount of pre-tightening selected lower than the proposed value leads to the joint loosening and shortened the bolt's fatigue life. Casanova and Mantilla [6] analyzed the failure of bolts employed to connect the turbine to the shaft of a hydroelectric power generator. Three of the ten bolts were broken during the disassembly process for replacing the turbine. The results showed that some of the scratches in the roots of the thread produced during the machining process and then corrosion during the working operation significantly have affected fatigue life. Zhu et al. [7] studied the failure analysis in the connecting rod cap and the connecting bolts of reciprocating compressor that were exposed to complex dynamic loads. Numerical and experimental results have demonstrated that reason of fatigue fracture was in high cycles. The initial crack location was consistent with the concentration of high stress in the curvature position of the connecting rod cap that before the connection of the bolts were broken. Molaei et al. [8] reviewed the failure of the sixteen connecting bolts of a filter press cylinder–piston system. They analyzed the state of bolt stress during service conditions, and the failure reasons were gathered from analysis of fracture and data. According to the results, it was concluded that due to insufficient torque applied to the bolts during assembly process, the bolts were damaged by fatigue mechanism. Kong et al. [9] analyzed the broken U-shaped bolts during the vehicle test. The cause of failure was studied using the tests of dimensional, macro–micro observations, metallographic, hardness and tensile property. The results showed that U-shaped bolts and nuts were imposed by fatigue fracture. The failure of the U-shaped bolts and nuts was due to the presence of densely distributed surface micro-cracks, small dimensions, surface decarburization appearance and low strength of materials. Qiu et al.

[10] analyzed the three main factors of bolt connections in slewing bearings by orthogonal design. They showed that the preload impact and the height of the bushes were more important than the friction coefficient of the contact surface between the bolt and the connection part. Jeong et al. [11] analyzed the processes of joining and releasing of bolt in joining bolts with different thickness and strength using finite element method. Their results indicated that in order to resolve of thread failure, the depth of connection should be chosen as low as possible. Pilone et al. [12] analyzed the failure of the bolt connections used to hold the lights in the tunnels of a highway. Studies indicated that failure is due to a deep corrosion process, with sodium chlorides sprayed inside tunnels during the winter to prevent freezing of the road. Studies also showed that corrosion only affects the bolts, while all other components of the joints were intact. The EDS analysis showed that stainless steel bolts were the copper type which did not have a relatively good corrosion resistance.

In most of the previous studies, the focus was on evaluating the determination of stress concentration points and the investigation of the microstructure of the bolt material, but the effect of the stress field on the fatigue life of bolt is a discussion that has not been considered very much. In summary, the innovations and objectives of the current study can be expressed as follows:

- Estimating the fatigue life of the bolts under the influence of stress fields with real geometry and comparing with the actual fatigue life of the broken bolts.
- Preparing experimental measurements on failure analysis including mechanical properties (hardness and tensile test), chemical composition of material and material microstructure using optical microscope (OM) and fractography of fracture surface by using scanning electron microscope (SEM) equipped with energy-dispersive spectrometry (EDS).
- Analyzing the failure causes and providing solutions to improve fatigue life.

2 Experimental work review method

The geometric dimensions are measured with the Micrometer and Vernier Caliper of the Mitutoyo Corporation of Japan. The accuracy of the Micrometer and the Vernier Caliper is 0.01 mm and 0.05 mm, respectively. Macroscopic observations are done using a Samsung 8MP AF camera with a 1.22-μm pixel size.

The chemical composition of the cylinder head bolt is examined according to ASTM E415-14 [13] and ASTME1086-14 [14] standards by SPECTROMAXx manufactured in Germany.

To examine the hardness and microstructure, a cross section of bolt with thickness of 15 mm is cut by the wire-cut EDM machine and then is machined from both sides. Grinding is done using sandpapers no. 60 to no. 1200, and fine polishing is used by diamond paste. Washing in alcohol and drying in hot air are used as the final step of finishing. Microstructure revealing, immersion etching is performed using aqueous solution of Nital 2%. Then, microscopic images are made using optical microscope (OM) from different areas of the bolt cross section. Finally, hardness test is performed using a hardness measurement device under 30 kg applied force for 10 s according to ASTM: E384-11e1 [15] standard.

For evaluating the mechanical properties of the bolt material, such as ultimate stress (US), yield stress (YS) and elongation, the samples are machined by a CNC lathe. The samples are then tested in accordance with the ASTM E8M-97a [16] standard and Ref. [17–20] by test machines. The results of the experiment are stored at the sampling rate of 2 times per second in the form of force–displacement. The length variation of the specimens is measured by an extensometer with a length of 50 mm. In order to perform the test, the motion speed of the machine grips is set at 0.50 mm.min^{-1}.

For investigation of the fracture surface, the broken bolts are first cut by an EDM machine and the samples are placed in an ultrasonic bath for one hour, and then, images are made with high magnifications by SEM machine model LEO 145 OVP having EDS model 7335. EDS is able to measure the chemical composition of the base material and impurities inside and around the crack zone.

Fatigue crack growth tests were carried out using three compact tension (CT) specimens and to prepare the CT specimens were carried out according to The ASTM E647-11 [21] standard. The CT specimens were subjected to constant amplitude fatigue loading under stress ratio $R = \sigma_{\min}/\sigma_{\max} = 0.83$. Fatigue cycling was sinusoidal with a frequency of 10 Hz.

3 Results and discussion

In this research, studying of engine cylinder head bolt failure in the features of this engine is shown in Table 1. Figure 1 indicates the fracture location of the bolts threads.

3.1 Material properties of cylinder head bolt

The chemical composition of the material forming component of the broken cylinder head bolt is listed in Table 2, in comparison with the applicable standard characteristic, in percentage by weight. The values of the elements specified in Table 2 are equivalent to DIN1.7034 steel in the DIN EN 10083-3:2007-01 [22] standard.

Table 1 Engine specifications and conditions

1	Engine configuration	4 stroke- cycle, petrol
2	Displacement (cc)	1800
3	Bore × stroke (mm)	81.4 × 83
4	Max. power (hp/rpm)	100/4250
5	Max. torque (kg.m/rpm)	14/4000
6	Cooling type	Water cooling
7	Combustion type	Multi-point injection (MPI)
8	No. of cylinder	4 in-line
9	Firing order	1–3–4–2
10	Compression ratio	9.4:1

Fig. 1 Photograph of the broken down three bolts at the threads

The mechanical properties of the cylinder head bolt material compared to the applicable standard specifications are listed in Table 3. The first to forth row of Table 3 shows average values of the three examined samples. Figure 2a shows the results of tensile tests at 24 °C (ambient temperature), and Fig. 2b shows the results of tensile tests at 24 °C, 200 °C, 300 °C and 400 °C temperatures, respectively. Because of better graphs representation and unnecessary for high strains in the present work, they are plotted at high magnification and up to 1% strain as Ref. [20]. Also, the value obtained from the tensile test at ambient temperature is within the equivalent standard characteristics to steel DIN1.7034/37Cr4.

Figure 2a, b show a proof which demonstrates that the mechanical strength of the material is significantly reduced by increasing the temperature, especially from the ambient temperature of 24–300 °C, as the tensile strength does not decrease minimally in the temperature range of 300–400 °C. The tensile strength at 400 °C is about 799 MPa, which is almost 70% of that at 24 °C.
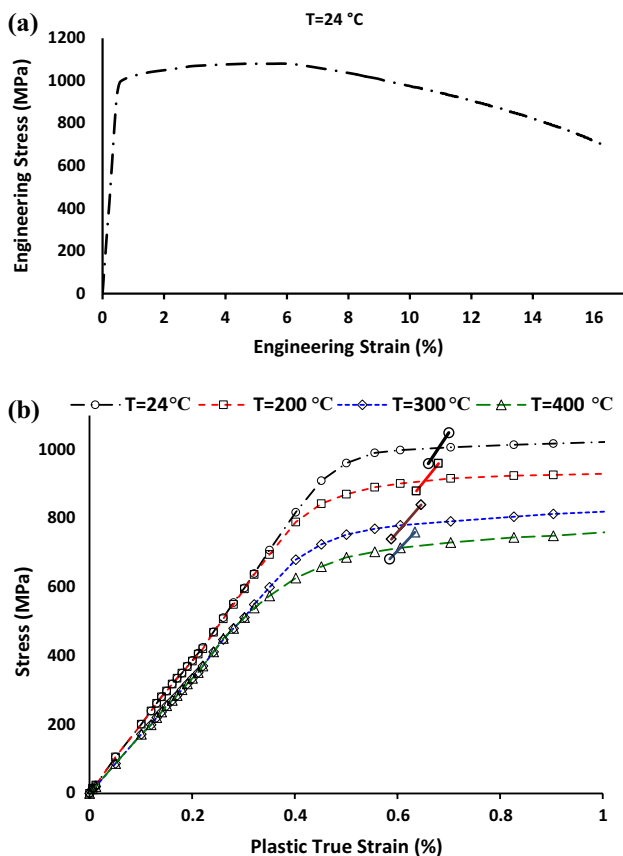
3.2 Hardness and micrographs

Figure 3a, b, respectively, show the micrograph of the sample cross section of the bolt and the thread, with a magnification of 50X by OM, and also Fig. 4a, b, respectively,

Table 2 The chemical composition of DIN1.7034 and DIN EN 10083-3:2007-01 [22] standard

Symbol	Fe	C	Si	Mn	P	S	Cr	Ni	Mo	Al	Cu
DIN1.7034	97.2	0.372	0.135	0.84	0.008	0.005	1.18	0.09	0.026	0.013	0.051
Standard	Base	0.34–0.41	≤ 0.040	0.60–0.90	≤ 0.025	≤ 0.035	0.90–1.20	–	–	–	–

Table 3 Mechanical properties of the DIN1.7034 and DIN [22] standard alloy

Symbol	Yield stress (MPa)	Ultimate tensile strength (MPa)	Temperature ($^{\circ}$C)
Sample 1	1005	1080	24
Sample 2	909	986	200
Sample 3	782	864	300
Sample 4	715	799	400
Standard alloy	Min. 750	950–1150	Ambient temp.

Fig. 2 a Engineering stress–strain curve of bolt material at 24 °C, and b the tested stress–strain curves of the bolt material at 24 °C, 200 °C, 300 °C and 400 °C with high magnification

show the micrograph of the sample cross section of the bolt and the thread, with a magnification of 1000X by SEM. In this images, the steel microstructure shows the

tempered martensitic type. The oxidized inclusions are found in great amounts on the etched areas in Figs. 3 and 4. For the inclusions investigation, the chemical composition by EDS is extracted from the sample cross section of the bolt and the thread, one of which is shown in Fig. 5. EDS examination of the sample cross section as shown in Fig. 5 reveals MgO and Al_2O_3 oxide inclusions. The presence of these inclusions according to Refs. [23, 24] is harmful to both the surface quality and forming properties of the final products. Also the presence of sharp oxide inclusions can cause stress concentration, which in turn results in crack growth due to the cyclic load of the combustion chamber pressure.

Figure 6a, b show the failed and sound threads micrograph of the bolt at 5X magnification, respectively. Figure 6a indicates thread corrosion effect that is related to the leak of the engine coolant resulted from the failure of the cylinder head gasket and cylinder head. One reason for premature failure of bolts is due to stress corrosion cracking (SCC) or localized pitting as indicated in Refs [25–28]. Corrosion depth is about 0.15 mm. Depth of corrosion can be one of the causes of fatigue crack initiation, but there are other causes as well as extra preload.

Then, hardness test is performed on the basis of the Vickers criteria according to the ASTM: E384-11e1 [15] standard and Bolts ISO: 898-1: 2009 (E) [29] standard on cross sections of the bolt and thread by hardness devices. First, a hardness test on the cross section of the specimen is performed with a force of 30 kg in 10 s and the hardness of the bolt center to the outer diameter of the bolt is plotted in Fig. 7. Then, hardness test is performed on three different threads on the wire cut specimen. The thread Vickers hardness is measured at points 1 and 2 of Fig. 7 in accordance with the requirements of Table 18 of ISO 898-1: 2009 (E) [29]. Molaei et al. [7] and Grimsmo et al. [30] obtained acceptable results for testing the bolt threads hardness using this standard. The test force is selected according to the standard 2.942 Newton (Vickers hardness test HV 0.3). The Vickers hardness value for a not carburize bolts at point 2 according to the standard should be greater than the Vickers hardness at point 1 in accordance with Eq. (1). For decarburization bolts:HV(2) ≥ HV(1) − 30 (1)

For decarburization bolts:HV$(2) \geq$ HV$(1) - 30$ (1)

In Fig. 7, the height of the not carburize E zone must be checked in accordance with ISO 898-1: 2009 (E). The

Fig. 3 Micrograph with 50X magnification; **a** bolt thread material, and **b** bolt cross section area material
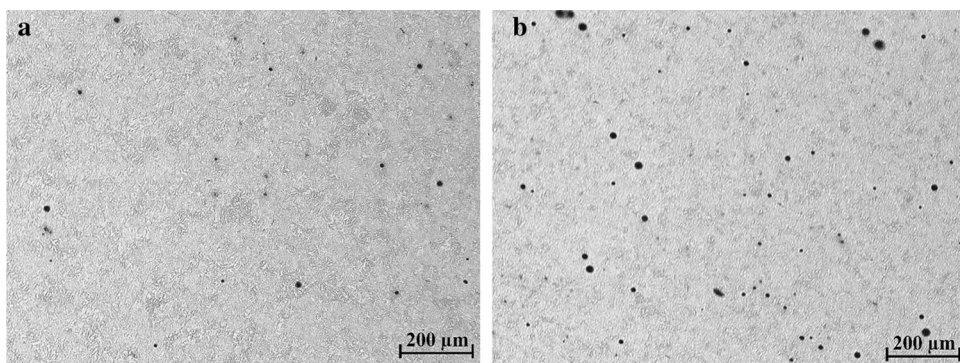

Fig. 4 Micrograph with 1000X magnification; **a** bolt thread material, and **b** bolt cross section area material
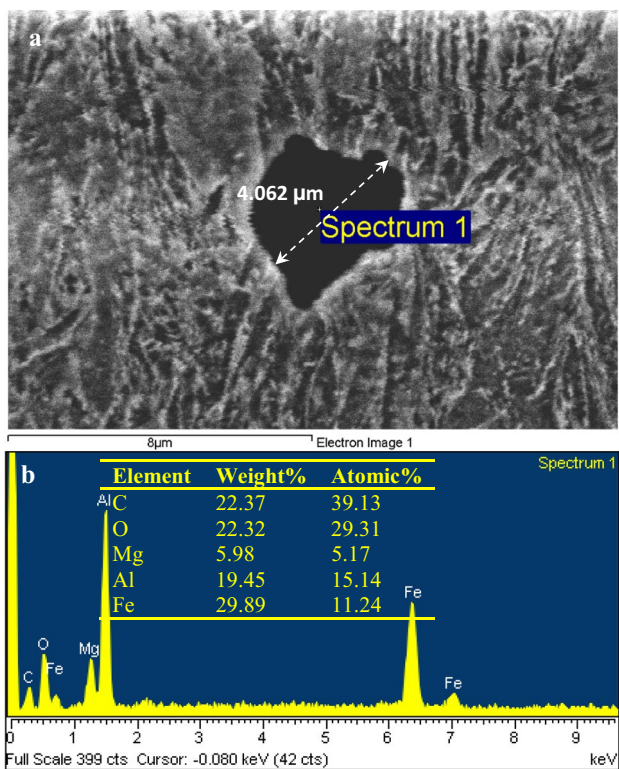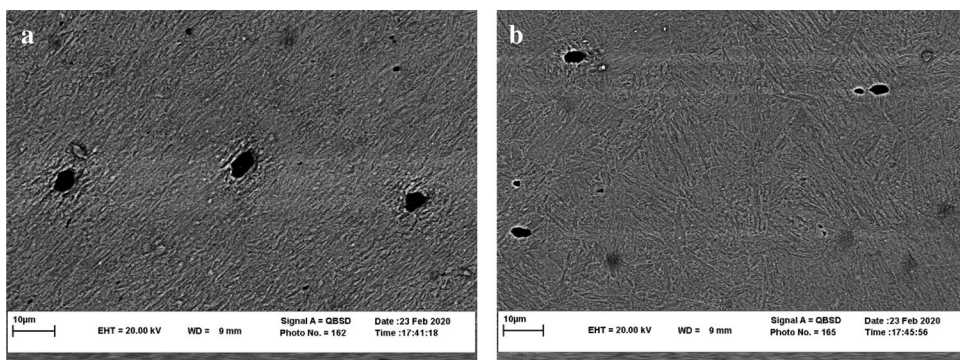

Fig. 5 Spectrum of impurity particle

measured hardness values of the threads are in accordance with the standard and are valid in Eq. (1). The results of Fig. 7 show that the bolt hardness increases from center to external diameter. The hardness values shown in Fig. 7 and the hardness values of the points 1 and 2 of Fig. 7 are within the bolts standard material, and therefore, the heat treatment performed on the bolts is correct and hardness is not observation any problem in the bolts.

3.3 Fractography of the fracture surface

The primary purpose of fractography science is finding the origin of the crack, and it is necessary for a proper analysis of the fracture. Initiation and propagation of the cracks would create the distinctive signs on the fracture surface, such as river signs, radial lines, chevrons and beachmarks that indicate the growth direction of the cracks. These marks are investigated for finding the origin of the cracks. The appearance of these marks on the crack surface is a function of tensile loading type, shear, bending, fatigue or torsional; stress state; amount of stress; existence of stress concentration; environmental factors and material factors [31, 32].

Figure 8 shows macro and micro views of the failed bolts. Figure 8a shows the macroscopic image of a broken surface of a cylinder head bolt that the morphology of the fracture

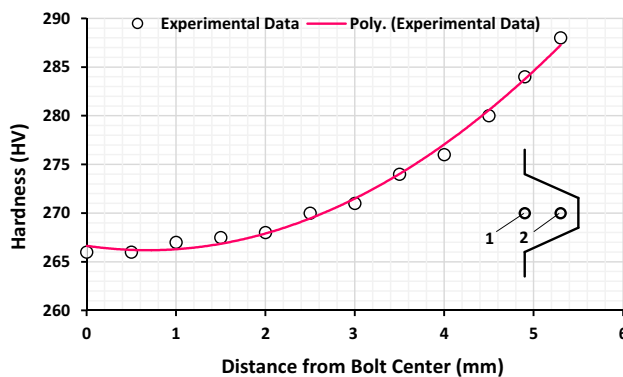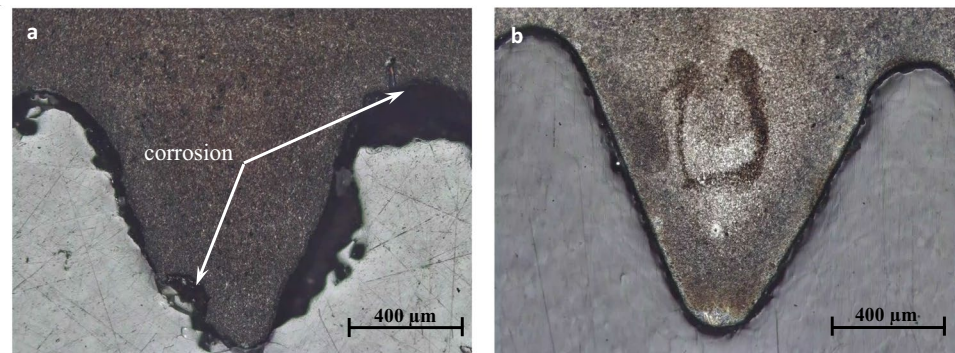**Fig. 6** Micrograph with 5×magnification; **a** failed thread, and **b** sound thread

Fig. 7 Hardness distribution from center to outer diameter of the bolt

surfaces shows region of ductile crack growth and crack initiation site (A), region of rapid crack growth indicated by presence of radial lines (B), the final fast fracture zone on to the opposite side of the crack initiation (C) and the direction of crack propagation in the region of rapid crack growth (arrow D). The magnitude of the final fast fracture zone (C) shows that loading is of high cycle stress type as indicated in Refs [32, 33]. For an accurate examination of the origins in prepared fracture surfaces, SEM images were used as shown Fig. 8b, c. Obvious fatigue characteristics of radial lines and beachmarks can be seen on the fracture surface, as shown in Fig. 8b. The image of the fracture surface by the SEM does not show a visible impurity. A large number of dimples are found in fracture extension area and short-break area, indicating that the toughness of the bolts is excellent as shown in Fig. 8c.

3.4 Stress analysis

The main components of an engine are the cylinders, coolant passages, oil galleries, crankcase and cylinder head. Figure 9 shows cylinder block, cylinder head and bolts of this case study in which cylinder head is attached to the cylinder block by bolts.

Cylinder head bolts must endure high loads to keep the cylinder head sealed tightly against the head gasket and block. Cylinder head bolts are loaded in tension due to the presence of pre-tightening force F_{PT}, maximum gas force F_G and force generated by the engine heat due to different temperatures F_T and different expansion rates of the cylinder block and the cylinder head. Figure 10 [3, 34] shows a diagram of force F versus deformation δ with a pre-tightening F_{PT}, regarding a cyclic loading F_G.

The bolt assembly process is one of the most important contributors to fatigue performance, but often overlooked. The cyclic stress amplitude imposed on a bolt is highly dependent on pre-tightening, because if the pre-tightening is increased there is a decreasing cyclic alternating stress σ_a. Lack of adequate pre-tightening promotes premature fatigue, leading to fatigue crack growth under service loading conditions. Table 4 lists calculations of proposed bolted joint and current work with details. Bowman [35] recommends a pre-tightening of 75% of proof load, which is about the same as the RB&W recommendations for reused bolts.

When the engine is in operation, the gas pressure leads to increase the length of the bolt which can cause deformation increase in the cylinder head and deformation reduction of the gasket. According to the 81.4 mm cylinder diameter (bore), the M11 × 1.5 bolt size, the 60 bar combustion pressure and the working temperature of the cylinder gasket at 200 °C, the pre-tightening stress σ_{minCW}, the pre-tightening stress plus stress amplitude σ_{maxCW} and the stress amplitude σ_{aCW} with the supplied data by Table 4 are 605.42 MPa, 729.96 MPa and 62.27 MPa, respectively. All three of these mentioned stresses should be lower than the proposed values, but in this study, the amount of pre-tightening stress is slightly higher than proposed pre-tightening load and the others do not have much difference.

Hence, one of the root causes of failure can be a deficient pre-tightening of the cylinder head bolts, which could originate a significant alternating stress amplitude. Bolts were going suffering some damage at the first threads, in the meantime aggravated by some corrosion. It is well known that cracks generally start at the threads fillet where
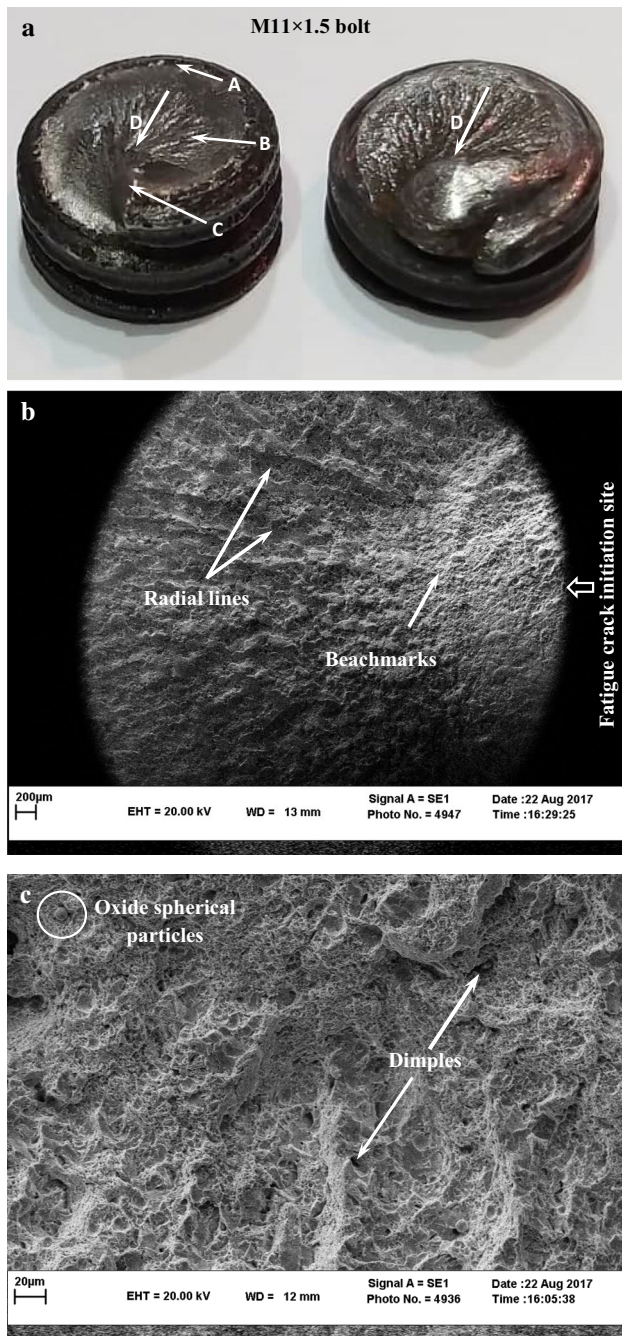
Fig. 8 Macro and micro views of the failed bolt; **a** Fracture surface of bolt (top), **b** SEM image of the A zone (middle), and **c** SEM image of the B zone (bottom)
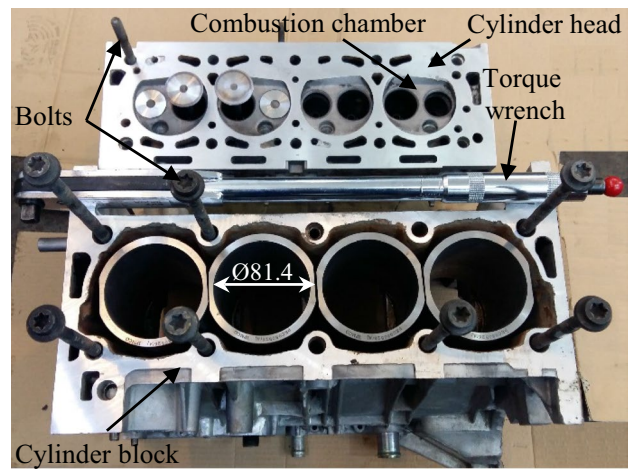

Fig. 9 **a** Cylinder head with six round nuts inserted at six studs, and **b** two open cylinder heads each one with six studs

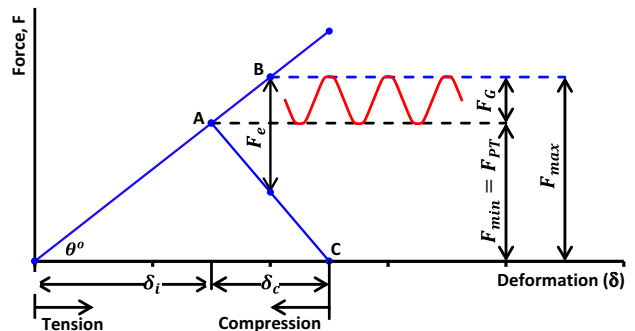**Fig. 10** Diagram representing the beneficial effect of a pre-tightening on bolts

the stress concentration is higher. One reliable indication is also revealed by the presence of beachmarks [32, 36], as is showed in this failure analysis. For all fractured cylinder head bolts the cycles to failure number of which is approximately 2×10^8, the root cause is the same.

3.5 Investigation of SIFs

Given that most cracks formed in the bolts are semi-elliptical shape, as in Fig. 11, the points on the crack front are at the deepest depth A of the crack, and where the cracks intersect with the outer surface (points B and C) the most important of them. The semi-elliptical axes are experimentally obtained according to the equation $b = 2s/\pi$ [37, 38] and Eq. (2) is extracted.

$$a = \frac{r \sin \theta}{\sqrt{1 - \frac{r^2}{b^2}(1 - \cos \theta)^2}} \tag{2}$$

The main field of research of fracture mechanics is the determination of stress intensity factors (SIF). In this study, the SIF, which is obtained from current work stress for mode I along the crack front of semi-elliptical surface cracks normal to the axis placed in the under tensile bolts, is determined by finite element analysis [39]. The total

Table 4 Calculations of proposed bolted joint and current work [3, 34]

|	Proposed	Current work
Preload	$F_{\min P} = F_{PT} = 0.75\,F_P = 39955.66\,\text{N}$	$F_{\min CW} = F_{PT} = \frac{T}{K \times d} = \frac{90000}{0.2 \times 10.78} = 41743.97\,\text{N}$
Maximum load	$F_{\max P} = F_P = 53274.22\,\text{N}$	$F_{\max CW} = F_{PT} + F_G = 50330.57\,\text{N}$
Alternating load	$F_{aP} = \frac{F\max_P - F\min_P}{2} = 6659.28\,\text{N}$	$F_{aCW} = \frac{F\max CW - F\min CW}{2} = \frac{F_G}{2} = 4293.3\,\text{N}$
Preload stress	$\sigma_{\min P} = \sigma_i = 0.75\,S_P = 579.49\,\text{MPa}$	$\sigma_{\min CW} = \frac{F\min CW}{A_t} = 605.42\,\text{MPa}$
Maximum stress	$\sigma_{\max P} = S_P = 772.65\,\text{MPa}$	$\sigma_{\max CW} = \frac{F\max CW}{A_t} = 729.96\,\text{MPa}$
Alternating stress	$\sigma_{aP} = \frac{\sigma\max_P - \sigma\min_P}{2} = 96.58\,\text{MPa}$	$\sigma_{aCW} = \frac{\sigma\max CW - \sigma\min CW}{2} = 62.27\,\text{MPa}$
Considerations	Minor diameter $d_r = d - 1.226869\,p = 10.78 - 1.226869 \times 1.5 = 8.94\,\text{mm}$	
	Mean diameter $d_m = d - 0.649519\,p = 10.78 - 0.649519 \times 1.5 = 9.8\,\text{mm}$	
	Effective tensile stress area $A_t = \frac{\pi}{4}\left(\frac{d_m + d_r}{2}\right) = \frac{\pi}{4}\left(\frac{d_m + d_r}{2}\right) = 68.95\,\text{mm}^2$	
	Proof Stress $S_P = 0.85 \times S_y = 0.85 \times 909 = 772.65\,\text{MPa}$	
	Proof Load $F_P = S_P \times A_t = 833 \times 68.95 = 53274.22\,\text{N}$	
	Cylinder area $A_{Cyl} = \frac{\pi d_{Cyl}}{4} = \frac{\pi \times 81.4^2}{4} = 5204\,\text{mm}^2$	
	Pre-tightening $F_{PT} = \frac{T}{K \times d} = \frac{90000\,\text{N.mm}}{0.2 \times 10.78} = 41743.97\,\text{N}$	
	Combustion force per bolt $F_G = \alpha\frac{P_G A_{Cyl}}{i} = 1.1 \times \frac{6 \times 5204}{4} = 8586.6\,\text{N}$	
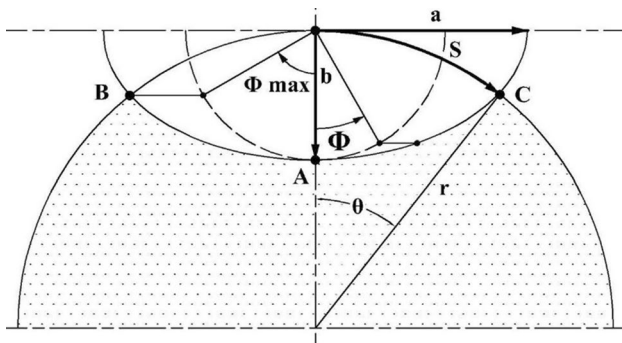
Fig. 11 Geometry of semi-elliptical surface crack

length of the arc crack 2 s as the crack parameter obtained from the broken bolt during the work in fatigue load is selected according to the methods of Shiratori et al. [40] and Freitas et al. [30]. Therefore, the stress intensity factors K_I for each point along the surface crack length are obtained by Eq. (3).

$$K_I = F_I\left(\frac{b}{r} \cdot \frac{b}{a} \cdot \varnothing\right) B_s \sqrt{\pi s} \tag{3}$$

That B_S is the applied tensile stress, s is the length of the half-arc crack, and F_I is the boundary correction factor, or SIF is the dimensionless state I, which is a function of the semi-ellipse crack form (b/a), the relative depth of the crack (b/r) and the position points along the front of the crack defined by the parametric angle $\varnothing$, as shown in Fig. 11,

which is determined according to the FEM calculations presented in [39].

In the present article, the SIFs of surface cracks in the bolt are deduced from the results of the stress analysis of finite element using the virtual crack extension method (Parks, 1974; Hellen, 1975). To simulate crack growth based on the measurement of half ellipses created at the broken surface of bolt, the finite element code has been used [41, 42]. In this study, the geometry of the crack is placed in semi-elliptical and on the plate that obtained in the stress analysis. The initial length of crack was investigated for five different cracks with dimensions of 0.1, 0.25, 0.35 and 0. 5 mm, which was considered as the initial crack. After loading, the workpiece is meshed, and then, the stress analysis is performed. Then, the SIF values are calculated. With the presence of SIFs values, crack growth direction is indicated. Crack growth was done manually, which in this method the amount of crack growth was desired. But it should be noted that the growth of the crack should not be more than 30% of the total length of the previous cracks. After crack growth, the workpiece is re-meshed and prepared for solution; this work should be repeated for each stage of growth of the cracks. The growth of the cracks continues to 14 stages, to reach of critical length 38 mm. As a result, the intensity of stress in 14 steps in front of the crack was studied for each stage of growth of the crack. Figure 12 shows the normalized SIF in s/s_m (s = curvilinear abscissa, s_m = arc length AB according to Fig. 11) for five cracks with dimensions of 0.1, 0.25, 0.35 and 0.5.

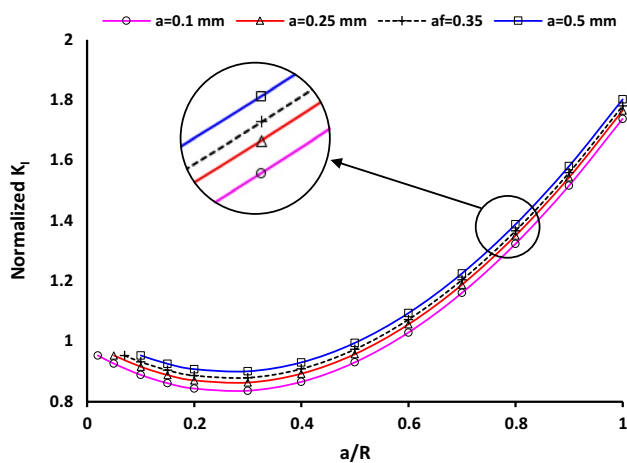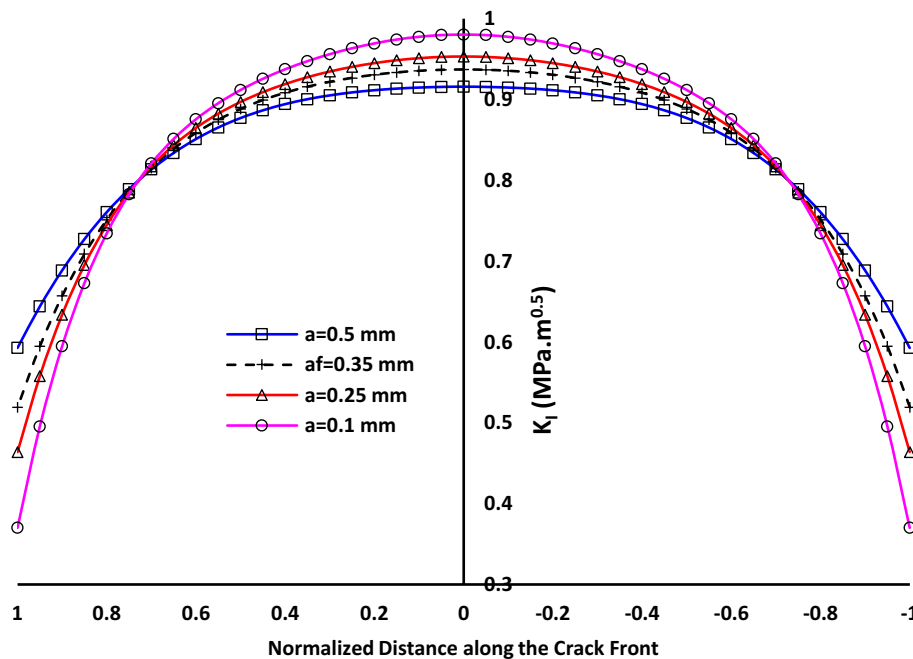**Fig. 12** Normalized SIFs along the crack front s/s_m

Fig. 13 Normalized SIFs versus the relative crack depth under tension

Fig. 14 Stress intensity factor range versus crack growth rate with stress ratio $R = 0.83$

The results obtained for the equivalent SIF at the tip of the crack are shown in Fig. 13. Based on Fig. 13, the maximum SIFs belong to the crack with longer length. As can be seen, whatever the length of the crack increases, the difference in the values of SIFs increases. In accordance with the relationship of Paris with the increase in the crack length, the rate of crack growth also increases. In other words, the difference of SIFs for crack with an initial length of 0.5 mm is much higher than the difference in the crack at the initial length of 0.1 mm.
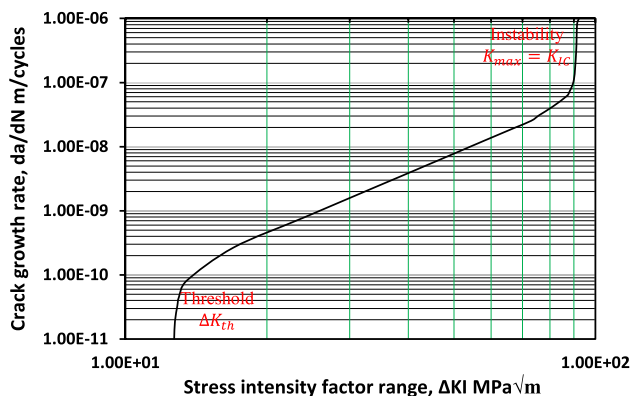
3.6 Evaluation of fatigue life

Then, after entering the necessary information and calculating the SIF values, the fatigue life for the desired bolt is calculated. Existing relationships in Refs. [43–45] can be used to obtain the growth rate of crack and fatigue life. In this study, the modified equation of Paris is used, which is applied effects from of the crack tip closure. The growth rate is defined by this equation as follows [46]:

$$\frac{\mathrm{d}a}{\mathrm{d}N} = C\left(\Delta K_{\mathrm{eff}}\right)^n = C\left(K_{\max} - K_{\mathrm{op}}\right)^n \tag{4}$$

For mode I loading, ΔK_{eff} is equal to ΔK_I which in Eq. (4), ΔK_{eff} is the effective SIF and is equal to the

difference between the maximum SIF $K_{\max}$ and the SIF value corresponding with opening stress, K_{op}. The coefficients C and n in this equation are the material constants, in which $n = 3.12$ and $C = 3.89 \times 10^{-14}$m/cycle in this study are extracted from Fig. 14. Also, the crack opening function, f, for plastic actuation of crack closure by Newman has been defined as follows [47].

$$f = \frac{K_{op}}{K_{\max}} = \begin{cases} \max\left(R, A_0 + A_1 R + A_2 R^2 + A_3 R^3\right) & R \geq 0 \\ A_0 + A_1 R & -2 \leq R < 0 \end{cases} \quad (5)$$

The above-mentioned coefficients are obtained from the following relationships:

$$A_0 = \left(0.825 - 0.34\alpha + 0.05\alpha^2\right)\left[\cos\left(\frac{\pi}{2}S_{\max}/\sigma_0\right)\right]^{\frac{1}{\alpha}} \quad (6)$$

$$A_1 = (0.415 - 0.071\alpha)S_{\max}/\sigma_0 \quad (7)$$

$$A_2 = 1 - A_0 - A_1 - A_3 \quad (8)$$

$$A_3 = 2A_0 + A_1 - 1 \quad (9)$$

In these equations, α is a constraint coefficient for the state of plane stress/strain, $S_{\max}/\sigma_0$ is the ratio of maximum applied stress to flow stress (required stress for the plastic flow creation), and R is the ratio of stress to each load cycle.

The number of cycles required for the growth of the crack from the initial length, a_0, to the final length, a_f, can be calculated using the following integral equation:

$$N_{tot} = \int_{a_0}^{a_f} \frac{\mathrm{d}a}{C\left(\Delta K_{eff}\right)^n} \quad (10)$$

where a_0 and a_f are the initial and the critical crack depths. The value of critical size, a_f, can be estimated by substituting where $a = a_f$, $\Delta\sigma = \sigma_{\max}$, which is the applied maximum tensile stress, $\Delta K_I = K_{IC}$, which is the fracture toughness of the material, and Y, which is the geometry factor, as follows Eq. (11) and Eq. (12) [48, 49]:

$$\Delta K_I = Y\Delta\sigma\sqrt{\pi a} \quad (11)$$

$$a_f = \frac{1}{\pi}\left(\frac{K_{IC}}{Y\sigma_{\max}}\right)^2 \quad (12)$$

Using $K_{IC} = 91.42$MPa$\sqrt{m}$, $\sigma_{\max} = 729.96$MPa and the approximate value of $Y = 1.107$ for the observed crack on the fracture surface is found to be $a_f = 3.98$mm.

During fatigue crack propagation, $\Delta K_{eff} = \Delta K_I$ value initially decreases until reaching a local minimum and then increases. If this local minimum value is less than

or equal to the threshold effective stress intensity factor range ($\Delta K_I < \Delta K_{eff\cdot th}$), the crack will not propagate. Conversely, if this local minimum value is greater than ΔK_{th} ($\Delta K_I > \Delta K_{eff\cdot th}$), crack propagation will continue until fracture. These relationships formed the basis for determining the threshold stress intensity factor range (ΔK_{th}) [50]. Given the value of $K_{th} = 12.9$ MPa$\sqrt{m}$ extracted from Fig. 14 and the value of the applied stress, the crack length equivalent to K_{th} is found to be $a_{th} = 0.13$ mm, and therefore, the lower value 0.1 mm is also be calculated.

Figure 15 shows the fatigue life in terms of the crack length for different values of the crack initial length. As can be seen, fatigue life also decreases by cracks length increment.

According to the results obtained for the fatigue life of the bolt, it can be figured out that the slope of the fatigue life curve is negligible per crack length. In other word, an insignificant increase in the crack length causes maximum fatigue life. Therefore, the SIF on the short cracks length is much more important than the SIF in longer cracks. Similar investigations (e.g., [51, 52]) have been reported the effect of increasing the initial crack length on increasing trend of fatigue life in rail wheels and crankshafts. Also, the results of Fig. 15 indicate that the being of crack with depth of 0.35 mm is the source of premature failure. One reason for premature failure of bolts is due to stress corrosion cracking (SCC) or localized pitting as indicated in Fig. 6a. Depth of corrosion can be one of the causes of fatigue crack initiation, but there are other causes as well as high pre-tightening stress.

4 Conclusions and suggestions

In this study, analysis investigation of fatigue failure was performed on cylinder head bolts. The failure after applying nearly 2×10^8 cycles in service in the zone of the cylinder head bolts threads of the gasoline engine is
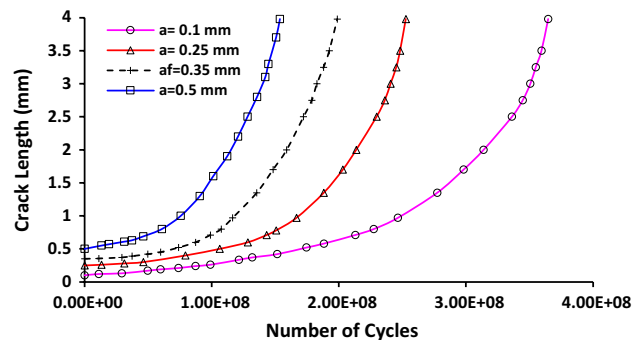

Fig. 15 Initial crack length influence on fatigue life

investigated. In this paper, mechanical properties (tensile and hardness test), chemical composition, microstructure and fractography are determined first. Exact prediction of fatigue crack growth on cylinder head bolts by experimental analysis and finite element method modeling can affect the Maintenance Planning and Scheduling Implementation. The main results of the present study could be expressed as following:

- Considering the results of the tensile test, the bolts are in the majority of the 10.9 Grade, that means the minimum ultimate strength is 1080 MPa, the yield strength minimum is 1005 MPa, and the minimum change of length (9%), as well as the chemical composition bolt Grade 10.9 is confirmed.
- The investigation with optical microscope showed that the microstructure of the steel is tempered martensitic type and conforms to the standard material.
- The morphology of fracture surface by optical and scanning electron microscopes shows the fatigue crack growth marks, including the radial lines and beachmarks.
- Numerical results show that crack to depth of 0.35 mm due to improper pre-tightening and corrosion effect is the source of failure of premature fracture.
- Regarding the type of loading, it is recommended that the correct torque be used to tighten the bolts and replace the bolts in each time cylinder head repair. Also, arrangements to prevent leakage of the coolant are being considered for decreasing corrosion effect.

References

1. Nami A, Aliakbari K, Ahmadipoor M, Mahdiloo AR (2019) Failure analysis of gasoline engine cylinder head bolts. In: 4th national conference in materials engineering. chemical engineering and industrial safety
2. Gong Y, Ding Q, Yang ZG (2019) Failure analysis on premature fracture of anchor bolts in seawater booster pump of nuclear power plant. Eng Fail Anal 97:10–19
3. Fonte M, Reis L, Infante V, Freitas M (2019) Failure analysis of cylinder head studs of a four stroke marine diesel engine. Eng Fail Anal 101:298–308
4. Yu Z, Xu X (2006) Failure analysis of diesel engine cylinder head bolts. Eng Fail Anal 13:826–834
5. Aliakbari K (2019) Failure analysis of base plate bolts of radial forging machine. J Stress Anal 4(1):89–98
6. Casanova F, Mantilla C (2018) Fatigue failure of the bolts connecting a Francis turbine with the shaft. Eng Fail Anal 90:1–13
7. Zhu X, Xu J, Liu Y, Cen B, Lu X, Zeng Z (2017) Failure analysis of a failed connecting rod cap and connecting bolts of a reciprocating compressor. Eng Fail Anal 74:218–227
8. Molaei SH, Alizadeh R, Attarian M, Jaferian Y (2015) A failure analysis study on the fractured connecting bolts of a filter press. Case Stud Eng Fail Anal 4:26–38
9. Kong H, Liu D, Jiang T (2015) U-shaped bolts fracture failure analysis. Procedia Eng 99:1476–1481
10. Qiu M, Yan J, Zhao B, Chen L, Bai Y (2012) A finite-element analysis of the connecting bolts of slewing bearings based on the orthogonal method. J Mech Sci Technol 26(3):883–887
11. Jeong JH, Lee HK, Park K, Kim JB (2015) An investigation into the anti-releasing performance of a serrated bolt. J Mech Sci Technol 29(12):5127–5132
12. Pilone D, Brotzu AA, Felli F (2015) Failure analysis of connecting bolts used for anchoring streetlights of a mountain highway. Eng Fail Anal 48:137–143
13. ASTM E415–14 (2014) Standard test method for analysis of carbon and low-alloy steel by spark atomic emission spectrometry. ASTM International, Philadelphia
14. ASTM E1086–14 (2014) Standard test method for analysis of austenitic stainless steel by spark atomic emission spectrometry. ASTM International, Philadelphia
15. ASTM E384–11e1 (2011) Standard test method for knoop and vickers hardness of materials. ASTM International, Philadelphia
16. ASTM A370–97a (2001) Standard test methods, and definitions for mechanical testing of steel products. ASTM International, Philadelphia
17. Aliakbari K, Farhangdoost KH (2014) Plastic deformation influence on material properties of autofrettaged tubes used in diesel engines injection system. J Press Vessel Technol 136:041402-1–041402-6
18. Aliakbari K, Farhangdoost KH (2014) The investigation of modelling material behavior in autofrettaged tubes made from aluminium alloys. Int J Eng 27:803–810
19. Zhang Q, Zuo Z, Liu J (2013) Failure analysis of a diesel engine cylinder head based on finite element method. Eng Fail Anal 34:51–58
20. Kılıçaslan C, İnce U (2016) Failure analysis of cold forged 37Cr4 alloy M10x28 bolts. Eng Fail Anal 70:177–187
21. ASTM E647-11 (2011) Standard Test Method for Measurement of Fatigue Crack Growth Rates. ASTM Int 3:1–46
22. DIN EN 10083-3:2007-01 (2007) Steels for quenching and tempering-Part 3: technical delivery conditions for alloy steels
23. Park JH, Kim DS (2005) Effect of CaO–Al_2O_3–MgO slags on the formation of MgO–Al_2O_3 inclusions in ferritic stainless steel. Metall Mater Trans B 36:495–502
24. Lyu S, Ma X, Chen M, Huang Z, Yao Z, Wang G, Zhao B (2020) Application of phase equilibrium studies of CaO–SiO_2–Al_2O_3–MgO system for oxide inclusions in Si-deoxidized steels. Calphad 68(101721):1–8
25. Yuan H, Liu H, Ren X, Zhang X, Ai D, Luo Y (2019) The bearing performance of the bolt-sphere joints with stochastic pitting corrosion damage. J Constr Steel Res 160:359–373
26. Craig P, Serkan S, Hagan P, Hebblewhite B, Van-dermaat D, Crosky A, Elias E (2016) Investigations into the corrosive environments contributing to premature failure of Australian coal mine rock bolts. Int J Min Sci Technol 26:59–64
27. Wu S, Chen H, Lamei H, Hagan PC, Hebblewhite B, Crosky A, Saydam S (2018) Investigation of cable bolts for stress corrosion cracking failure. Constr Build Mater 187:1224–1231
28. Wu S, Chenb H, Craiga P, Ramandia HL, Timmsa W, Hagana PC, Crosky A, Hebblewhitea B, Saydama S (2018) An experimental framework for simulating stress corrosion cracking in cable bolts. Tunn Undergr Space Technol 76:121–132

29. ISO 898-1:2013 (en) (2013) Mechanical properties of fasteners made of carbon steel and alloy steel- Part 1: bolts, screws and studs with specified property classes—coarse thread and fine pitch thread

30. Grimsmo EL, Aalberg A, Langseth M, Clausen AH (2016) Failure modes of bolt and nut assemblies under tensile loading. J Constr Steel Res 126:15–25

31. Aliakbari K (2019) Failure analysis of four-cylinder diesel engine crankshaft. J Braz Soc Mech Sci Eng 41(1):30–41

32. American Society for Metals, and ASM International (1987) ASM Handbook. Vol. 12. https://doi.org/10.31399/asm.hb.v12.9781627081818

33. Aliakbari K, Safarzadeh N, Mortazavi SS (2018) Analysis of the crankshaft failure of wheel loader diesel engine. Int J Eng 31:473–479

34. Shigley's JE (2012) Mechanical Engineering Design, 9th edn. Mc-Graw-Hill, Chapter, p 8

35. Bowman Distribution-Barnes Group (1985) Fastener facts. Cleveland, Ohio

36. Infante V, Silva JM, Silvestre M, Baptista R (2013) Failure of a crankshafts of an aeroengine: a contribution for an accident investigation. Eng Fail Anal 35:286–293

37. Freitas MD, François D (1995) Analysis of fatigue crack growth in rotary bend specimens and railway axles, Fatigue Fract. Eng Mater Struct 18:171–178

38. Fonte M, Freitas M (1997) Semi-elliptical crack growth under rotating or reversed bending combined with steady torsion, Fatigue Fract. Eng Mater Struct 20:895–906

39. Fonte M, Freitas M (1999) Stress intensity factors for semi-elliptical surface cracks in round bars under bending and torsion. Int J Fatigue 21:457–463

40. Shiratori M, Miyoshi T, Sakay Y, Zhang GR (1987) Factors analysis and application of influence coefficients for round bar with a semi-elliptical surface crack. In: Murakami Y (ed) Handbook of Stress Intensity Factors, vol 2. Pergamon Press, Oxford

41. Hellen TK (1975) On the method of virtual crack extension. Int J Numer Meth Eng 9:187–207

42. Parks DM (1974) A stiffness derivative finite element technique for determination of elastic crack tip stress intensity factor. Int J Fract 10:487–502

43. Forman RG, Kearney VE, Engel RM (1976) Numerical analysis of crack propagation in cyclic-loaded structures. J Basic Eng 89:459–463

44. Elber W (1971) The significance of fatigue crack closure, in damage tolerance in aircraft structures. ASTM STP 486:230–242

45. NASA (2000) Fatigue Crack Growth Computer Program NAS-GRO Version 3.0, Reference Manual. JSC-22267B, NASA, Lyndon B. Johnson Space Center, Texas

46. Anderson TL (1994) Fracture Mechanics, fundamentals and applications, 2nd edn. CRC Press, Boca Raton

47. Newman JJ (1984) A crack opening stress equation for fatigue crack growth. Int J Fract 24(4):131–135

48. Murakami Y (1987) Stress intensity factors handbook, vol 1. Pergamon Press, Oxford

49. Mehrzadi M, Taheri F (2012) The influence of negative and positive stress ratios on crack growth rate in AM60B magnesium alloy. Mater Sci Eng, A 545:68–77

50. Fukumura N, Suzuki T, Hamada S, Tsuzaki K, Noguchi H (2015) Mechanical examination of crack length dependency and material dependency on threshold stress intensity factor range with Dugdale model. Eng Fract Mech 135:168–186

51. Masoudi Nejad R, Farhangdoost KH, Shariati M (2015) Numerical study on fatigue crack growth in railway wheels under the influence of residual stresses. Eng Fail Anal 52:75–89

52. Aliakbari K, Imanparast M, Masoudi Nejad R (2019) Microstructure and fatigue fracture mechanism for a heavy-duty truck diesel engine crankshaft. Sci Iranica B 26(6):3313–3324